Proceedings of DSCC 2008
ASME 2008 Dynamic Systems and Control Conference
October 20-22, 2008, Ann Arbor, Michigan, USA

DSCC2008-12345

NUMERICAL EVIDENCE FOR CUTOFFS IN CHAOTIC MICROFLUIDIC MIXING

Tzu-Chen Liang
Department of Aeronautics and Astronautics
Stanford University
Stanford, California 94305
Email: tzuchen@stanford.edu

Matthew West
Department of Mechanical Science and Engineering
University of Illinois at Urbana-Champaign
Urbana, Illinois, 61801
Email: mwest@uiuc.edu

ABSTRACT

Chaotic mixing strategies produce high mixing rates in microfluidic channels and other applications. In prior numerical and experimental work the variance of a tracer field in a chaotic mixer has been observed to decay rapidly after an initial slower transient. We relate this to the cutoff phenomenon observed in finite Markov chains and provide numerical evidence to suggest that chaotic mixing indeed exhibits cutoff. We provide results for a herringbone passive microfluidic mixer and the Standard Map.

INTRODUCTION

The question of how chaotic advection mixes a passive scalar function has attracted much research effort in recent years [1]. The main issues in this field are: how to measure the thoroughness of the mixing, how the mixing process changes qualitatively and quantitatively when the diffusion is close to zero, and how to enhance the overall mixing process by designing the map which produces chaotic advection. Unfortunately, we have only partial understanding for most of these topics. In spite of the fact that the detailed mechanism of mixing is unclear, non-trivial mixing processes have been observed in experiments [2] and can be simulated by large-scale computations [3].

A widely observed phenomenon in the chaotic mixing process when small diffusion exists is the two or three-stage transition [4–6]. The map does not mix the scalar function with a constant rate in general. When the variance of the scalar function is measured during the mixing process, one can in general observe a relatively flat decay initially, followed by a super-exponential change, and then finally it tends to an exponential decay. We are interested in when these transitions happen, why they happen, and how to predict the slope of the exponential region. A good review and physical interpretation can be found in [7].

Thiffeault and Childress [4] study these properties for a modified Arnold's cat map. Analytical formulas are given to predict the transitions as well as the slopes. Because the linear part of this map has an eigenvalue 2.618, which stretches very fast, and the chaotic part is relatively small, the three phases are separated clearly. The same analytical procedure cannot be applied to, for example, the Standard Map, although the only difference between the Standard Map and the modified Arnold's cat map is in the linear part.

As for the exponential decay part, there is still debate about whether the decay rate goes to zeros in the zero diffusivity limit or whether it tends to a constant independent of the diffusion [3, 7]. Theoretical analysis shows both of these possibilities can occur for different chaotic flows [8].

Difficulties typically arise in studying the above problems numerically, because the small diffusion usually means fine grids are required in the solution of the Advection-Diffusion equation or the simulation of the map. Some studies and numerical results conclude that a proportional relation exists between the stationary decay rate and the diffusion [9]. However, this is only true for certain diffusion ranges.

Our goal in this paper is to relate the chaotic mixing process to the well-known cutoff phenomenon in finite Markov Chain studies. We begin with a numerical simulation of a chaotic mixing channel. How well the different color liquids are mixed is measured by the color variance on the cross-sections of the channel. The simulation shows that when we increase the Péclet number, the mixing trajectory presents a cutoff. We then use a simple example–Baker's Map advects a sinusoidal function–to explain the physical mechanism to cause this. To support the chaotic mixing channel example, A very high resolution numerical simulation of Standard Map is then presented to show that in the near-zero diffusion limit, it does present a cutoff.

BACKGROUND

The measure space and operators

We work on the probability space $(X, \mathcal{A}, \mu)$. We take $S : X \to X$ to be a transformation (or map) that is non-singular and measurable. We choose μ to be the Borel measure. In the measure space $(X, \mathcal{A}, \mu)$ we define the following operators.

Definition 1. ***(Perron-Frobenius operator)*** *The Perron-Frobenius operator $P : L^1(X) \to L^1(X)$ associated with S satisfies*

$$\int_A (P\omega)(x)\mu(dx) = \int_{S^{-1}(A)} \omega(x)\mu(dx) \tag{1}$$

for every $\omega \in L^1(X)$ and $A \in \mathcal{A}$.

The Perron-Frobenius operator is linear. Because of our choice of measure space, the Perron-Frobenius operator can be interpreted as a map that evolves probability density functions. Also, suppose that $\bar{\omega}$ is an invariant measure of S, so that $\bar{\omega}(S^{-1}(A)) = \bar{\omega}(A)$ for all $A \in \mathcal{A}$. Then we have $P\bar{\omega} = \bar{\omega}$ (omitting x).

Definition 2. ***(Koopman operator)*** *Let $f \in L^\infty(X)$. The operator $U : L^\infty(X) \to L^\infty(X)$ defined by $Uf(x) = f(S(x))$ is called the Koopman operator associated with S.*

The Koopman operator is adjoint to Perron-Frobenius operator, which we write as $U = P^*$.

In the measure space $(X, \mathcal{A}, \mu)$, where μ is the Borel measure, let P_S and U_S be the Perron-Frobenius and the Koopman operators of an invertible map S. We have the following relations:

	forward in time	backward in time
probability density	P_S	$P_{S^{-1}}$
scalar function	$U_{S^{-1}} = P^*_{S^{-1}}$	$U_S = P^*_S$

Our goal is to simulate how a scalar function is advected by a chaotic map forward in time. From the above table, it is clear we should use the operator $U_{S^{-1}}$. For a given initial function $f^0(x)$, one has, $f^{k+1} = U_{S^{-1}} f^k$, for all k.

Numerical Strategy

Numerically, an approximation of $U_{S^{-1}}$ is used. For a map $S : X \to X$, we discretize X into regular square grids with size h. The grids are numbered as $a_1, a_2, .., a_n$. We first define a map (an observer) $g_n : f(x) \mapsto f_n$ such that

$$(f_n)_i = (g_n(f(x)))_i = \int_{a_i} f(x)\mu(dx), \text{ for } i = 1 \text{ to } n. \tag{2}$$

This g_n maps the scalar function we are interested into a finite length vector in $\mathbb{R}^n$, and thus we just need a linear operator $B_n : \mathbb{R}^n \to \mathbb{R}^n$ to approximate $U_{S^{-1}}$, and evolve the function in the reduced space $\mathbb{R}^n$. The B_n we use in our numerical simulation is obtained by a very simple way: let $\mathbf{x}_i = (x_{1i}, x_{2i})$ be the center of grid a_i, then define a matrix B_n as,

$$(B_n)_{ij} = \begin{cases} \frac{1}{4} & \text{, if } S(x_{1j} \pm \frac{h}{2}, x_{2j} \pm \frac{h}{2}) \in a_i, \\ 0 & \text{, otherwise.} \end{cases} \tag{3}$$

The matrix B_n has only 4 non-zeros in each row. For a given f^0, we can thus approximate equation the evolution by $f_n^{k+1} = B_n f_n^k$.

This approach is similar to the lattice method [3, 10]. We shall stress that there exists better approximations of $U_{S^{-1}}$ which minimize the difference between f_n^k and $g_n(f^k)$ [11] by applying optimal model reduction. However, our simple numerical strategy allows us to go up to very large n and to simulate the system with very small numerical diffusion. During the simulation matrix B_n is never explicitly formed. We need only store a size n state vector during the iteration. This approximation ensures the operation count of evolving the system is always a constant times n.

Using the above numerical strategy, we can evolve a function or a probability distribution by the map with some small numerical diffusion. The effect of numerical diffusion is similar to physical diffusion in large scale, but their behaviors can be quite different in small scale. To simulate the physical diffusion correctly, we need to simulate the map with far higher resolution with some additional diffusion added. The additional diffusion can be added by either in spatial or frequency domain. In spatial domain, we adopt the method of adding a smoothing step used in [3],

$$f^{k+1}_{(p,q)} = \sum_{|r|,|s| \le 2} C_{|r|} C_{|s|} f^k_{(p,q)} \tag{4}$$

with $C_0 = 1/8, C_1 = 1/4$, and $C_2 = 3/16$ and (p,q) is the 2-D index of a grid. This creates a large scale diffusion $D \approx h^2$, which is several times larger than the numerical diffusion we originally have [3]. We use a smoothing operator M_n and $f^{k+1} = M_n(f^k)$ to denote the above smoothing step and define $\bar{B}_n = M_n \circ B_n$.

Alternatively, in frequency domain a two dimensional FFT/IFFT with a multiplication of a constant in between according to the wave numbers can be applied to simulate physical diffusion, too. This procedure is denoted by an operator F_n, $f^{k+1} = F_n(f^k)$ and $\hat{B}_n = F_n \circ B_n$. Note the FFT/IFFT scheme is much more expensive when n is large.

Notion of a cutoff

In some Markov Chains, certain probability distributions converge to an equilibrium via a sharp transition, which becomes sharper for larger chains. This phenomenon is referred to as *cut-off* in the finite Markov chain literature [12]. Here we extend the usual definition slightly to accommodate converge to non-zero distance values.

To any finite set Ω and any pair of probability measures ω,

$\bar{\omega}$ on Ω we associate a real number $d(\omega,\bar{\omega})$ such that

$$d(\omega,\bar{\omega}) \in [0,1] \tag{5a}$$

$$d(\omega,\bar{\omega}) = 0 \text{ if and only if } \bar{\omega} = \omega \tag{5b}$$

$$\max_{\Omega,\omega,\bar{\omega}} d(\omega,\bar{\omega}) = M_d. \tag{5c}$$

Note that d need not satisfy the triangle inequality and so is not a metric.

Consider a sequence of finite probability spaces (Ω_n) for $n = 1,2,\ldots$. We think of n as the size of the space. Each space is equipped with a probability measure $\bar{\omega}_n$ which we think of as the unique invariant measure of a Markov chain on Ω_n. For each n we now take a sequence of probability measures ω_n^k for $k = 0,1,2,\ldots$ such that $\lim_{k\to\infty} d(\omega_n,\bar{\omega}_n) = 0$. The ω_n^k should be thought of as an initial condition ω_n^0 and then iterates of the distribution under the evolution of a Markov chain. The definition of a cutoff is,

Definition 3 (Cutoff). *Take a family $(\Omega_n,\bar{\omega}_n,(\omega_n^k)_{k=0}^{\infty})_{n=1}^{\infty}$ of finite probability spaces Ω_n and probability measures $\bar{\omega}_n$ and ω_n^k. This family presents a d-cutoff if there exists a sequence $(t_n)_{n=1}^{\infty}$ of positive reals such that, for any $\varepsilon \in (0,1)$,*

$$\lim_{n\to\infty} d(\omega_n^{k_n},\bar{\omega}_n) = m \text{ if } k_n > (1+\varepsilon)t_n \tag{6a}$$

$$\lim_{n\to\infty} d(\omega_n^{k_n},\bar{\omega}_n) = M \text{ if } k_n < (1-\varepsilon)t_n \tag{6b}$$

This definition is taken from [12] with the change that m and M are 0 and M_d in the original. The reason for this modification will be clear when we present the results of Standard Map simulation.

The definition of cutoff implies that the change of $d(\omega_n^k,\bar{\omega}_n)$ from M to m happens ever more rapidly as n increases, but only in relation to the cutoff times t_n. We can think of this as rescaling the each trajectory $(\omega_n^k)_{k=0}^{\infty}$ in time by t_n and seeing cutoff as the limit of these rescaled trajectories to a step function. We give an example of cutoff phenomenon:

Example 1. ***Random walk on an n-dimensional hypercube*** *(Diaconis [13]) a particle starts at $\mathbf{0}$ and moves to one of its nearest neighbors (or stay fixed) with equal probability at each step. The problem can be formulated as a Markov Chain with 2^n states and invariant distribution $\bar{\omega}$ is uniform. The $|\omega_n^k - \bar{\omega}|_{TV}$ (Total Variation Distance) versus iteration plot with different n is shown in figure 1.* ◊

How to tell a cutoff?

To prove cutoffs is in general very hard. It requires a lot of mathematical tools and very special features of the sequence of systems. However, people believe cutoffs happen more frequently than we thought. In this article we merely provide numerical evidence of cutoffs. The way we tell a sequence of simulation results presents a cutoff or not is through the definition. We first define a cutoff time t_n, it is usually the number of iterations required for the trajectory indexed by n to pass through

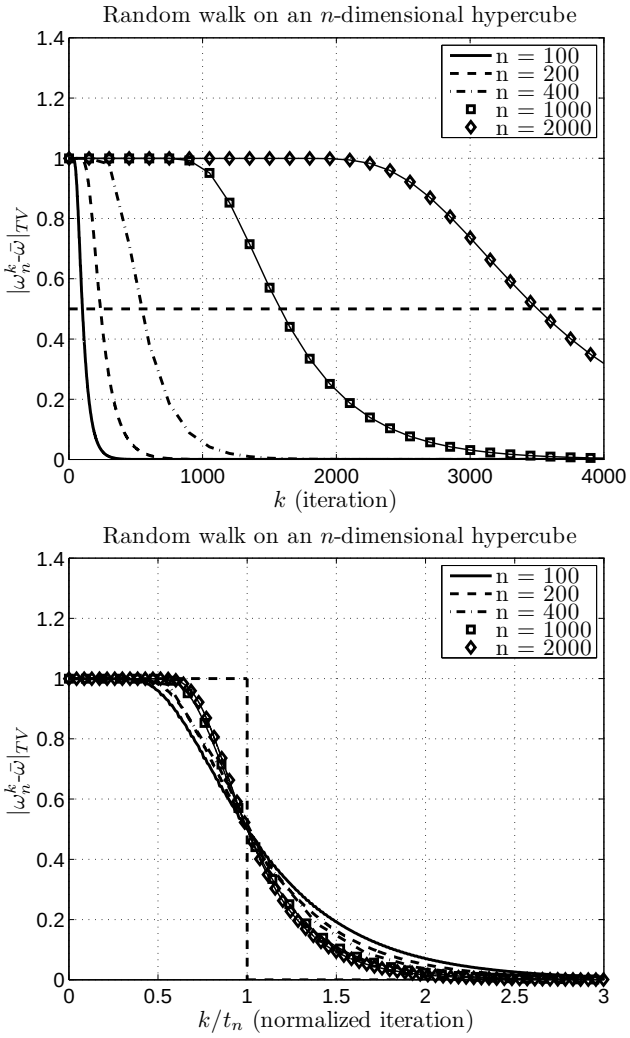

Figure 1. THE UPPER FIGURE SHOWS THE k VERSUS $|\omega_n^k - \bar{\omega}|_{TV}$ PLOT OF RANDOM WALK ON AN n-DIMENSIONAL HYPERCUBE PROBLEM. WHEN n INCREASES, THE DISTANCE STAYS CLOSE TO 1 FOR MORE ITERATIONS BEFORE IT DROPS TO ZERO. DEFINE t_n AS THE NUMBER OF ITERATIONS FOR $|\omega_n^k - \bar{\omega}|_{TV}$ TO BE LOWER THAN 0.5. IN THE BOTTOM FIGURE WE NORMALIZE THE TRAJECTORIES BY RESCALING THE HORIZONTAL AXIS BY t_n TO OBESERVE THE CUTOFF.

$(M_\star + m_\star)/2$, where $\star$ indicates the operator used in the simulation, and then all the trajectories are rescaled by their t_n on the iteration axis to normalize. If the normalized plot shows the tendency to converge to the function:

$$\beta_{\star_\infty}(x) = \begin{cases} M_\star & \text{, if } x < 1, \\ m_\star & \text{, otherwise,} \end{cases} \tag{7}$$

then one can tell this sequence of simulations presents a cutoff. One can see the second plot in figure 1 for an example. However, as we shall see clearly later, the difficulty to decide a cutoff numerically is it requires large-scale simulation to see this tendency clearly. Hence we provide a weaker way to justify the

convergence. We define the interpolating functions for the trajectories in the normalized plots to be $\beta_{\star_n}(x)$, where x represents the normalized iteration. Define the distance between $\beta_{\star_n}(x)$ and $\beta_{\star_\infty}(x)$ to be, $\Delta^l_\star$, and

$$\Delta^l_\star = \int_0^l |\beta_{\star_\infty}(x) - \beta_{\star_n}(x)| dx \tag{8}$$

We calculate $\Delta^3_\star$ for all $\beta_\star(x)$, and plot them versus t_n. This figure shows how $\Delta^3_\star$ decays when t_n increases, and it thus gives us the idea whether this sequence of simulations presents a cutoff.

The quantity people are interested in chaotic mixing is the variance of the function, and in the study of cutoff phenomenon, total variation distance is the object which is discussed the most. There is no difficulty to set the distance function $d(\omega, \bar{\omega})$ to be the 2-norm as the following:

$$d(\omega_n, \bar{\omega}_n) = \left(\sum_{i=1}^{n} \left(\frac{(\omega_n)_i}{(\bar{\omega}_n)_i} - 1 \right)^2 (\bar{\omega}_n)_i \right)^{1/2}. \tag{9}$$

This corresponds to the study of L_2 cutoff in the cutoff terminology.

It is clear that the maximal value of the 2-norm distance is ∞, so we need to set $M_d = \infty$ (in stead of $M_d = 1$ for total variation distance). In the original cutoff definition, (M, m) always equals $(M_d, 0)$, but in our examples we will set M to have a finite value (0.5 in the mixing channel case and 1 in the Standard Map case) which does not maximize the distance function.

THE MICROFLUIDIC MIXING CHANNEL

Microfluidic systems control and manipulate liquids in microliter or nanoliter amounts. One of the challenges in microfluidics is the design of mixing channels, whose objective is to thoroughly mix two or more different liquids. Although the mixers designed by using active components like micro-pumps to stir the flow have very promising results [14], passive mixing devices have advantages in manufacturing simplicity and price.

A microfluidic mixing channel typically has cross-section dimension $\ell \sim 100\mu m$, and Reynolds number $\mathrm{Re} = U\ell/\nu$ is less than 100 [15] (U is the average velocity of the liquid and ν is the kinematic viscosity of the fluid). Fluid flow on this scale is highly laminar and the mixing of materials between streams is purely diffusive. The dimensionless number that controls the length of the channel required for mixing is Péclet number ($\mathrm{Pe} = U\ell/D$ where D is the molecular diffusivity). For a pressure-driven mixing channel the mixing length can be expected to grow linearly with Pe and is usually much more than 1 cm. Hence various designs are proposed to stir the flow inside the channel and produce transverse velocities to enhance the mixing [15, 16].

Stroock, et. al [15] proposed a staggered herringbone mixer which is composed of two sequential regions of ridges; the direction of asymmetry of the herringbones switches with respect to the center-line of the channel from one region to the next. The herringbone structure is fabricated with two steps of photolithography and is located on the floor of the poly channel. Experiments show that the length of the channel required for mixing grows only logarithmically with Pe. The goal of the herringbone structure is to produce transverse flows, basically one large and one small vortices, and we further optimize in the structure [17] by using the techniques of topology optimization. The optimized half-cycle structure is shown in the figure 2, where $(\ell_x, \ell_y, \ell_z) = (0.06, 0.01, 0.02)$ cm. The same pattern repeats four times in the half-cycle structure. One full-cycle is composed of two half-cycle channels which arrange as in Strook's design.

We stimulate the mixing process of the proposed mixing channel by first solving the velocity field for one full-cycle of the mixing channel, and then defining an inlet-outlet flow map by integrating the streamlines. Once the flow map is obtained, we can apply our numerical strategy to simulate the mixing process. One should be notified that the actual mixing process happens in between the streamlines and is the solution of the Advection-Diffusion equation. We approximate this complicated process by the simple model outlined above, and lump all the diffusion happening inside the mixing channel into an FFT/IFFT diffusion operator F_n. Thus the operator to perform this simulation is $\hat{B}$.

In figure 3, the optimized mixing channel is used to perform the simulation with different Pe. We adjust Pe by changing the FFT/IFFT diffusivity between each full-cycle (0.12 cm). The trajectories have the same tendency as the experiment results in the figure 3(D) in [15]. Define mixing length (x_{90}) as the channel length required for the standard deviation to drop to 0.05 (shown by a dashed line in figure 3). The mixing length grows linearly with $\log(\mathrm{Pe})$, which also matches the experiments done in [15].

Let $n = \mathrm{Pe}$. Define t_n as the number of iterations required for each of the trajectories to pass through 0.25. The normalized plot is shown in the first plot of figure 4. One can see a cutoff clearly forming. The cutoff time versus Pe trajectory is shown in the second plot of figure 4. Just like x_{90}, the cutoff time grows linearly with Pe. The $\Delta^3_{\hat{B}}$ versus Pe plot is shown in the last plot of figure 4. The decreasing trajectory implies that the normalized trajectories is likely to form a cut eventually.

Figure 5 we show some cross-sectional plots of two of the simulations in figure 3, where Pe are 1.2×10^6 and 1.2×10^9, respectively. The first four plots of each case show the cross-section at the end of the 1st to the 4th cycle, and the last plot for each case shows the cross-section at the end of the 9th cycle. From this comparison one can clearly see how the chaotic mixing protocol helps color mixing even when diffusion is very small.

More detail about this simulation can be found in [17]. In this article, we are more interested in characterizing the trajectories shown in figure 3 by cutoff phenomenon. However, large Pe means fine grids and thus much more streamlines need to be calculated. Further increasing Pe and observing a clearer cutoff is prohibited by the computation power. Hence in the following two sections, we discuss two discrete chaotic maps and provide analytical and numerical evidence of cutoffs in chaotic mixing.

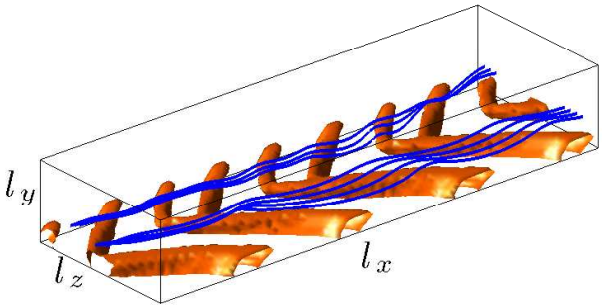

Figure 2. THE OPTIMIZED CHANNEL STRUCTURE TO PRODUCE ONE BIG AND ONE SMALL VORTICES.

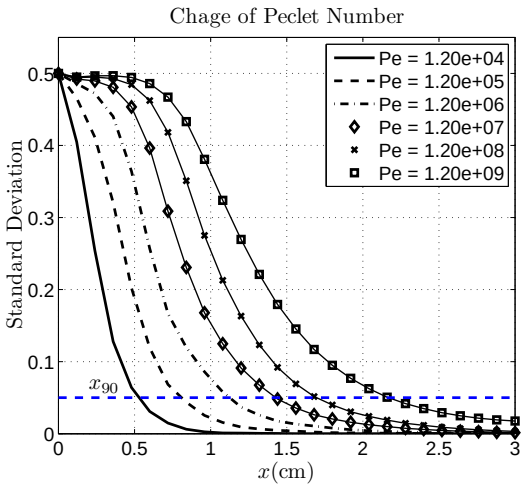

Figure 3. IN THIS FIGURE WE VERY Pe BY CHANGING by D AND USE OPTIMIZED HERRINGBONE STRUCTURED CHANNEL FOR SIMULATION. THE MIXING TRAJECTORIES STAYS ALMOST 0.5 FOR A LONGER DISTANCE WHEN Pe IS LARGE.

THE SUPER-EXPONENTIAL MIXING CURVE

In this section we use a simple example to explain why we expect to see the concave mixing trajectory in the beginning of a chaotic mixing process. Consider Baker's map on T^2:

$$S(x_1,x_2) = \begin{cases} (2x_1, \frac{1}{2}x_2) \bmod 1, & \text{if } 0 \le x_1 < \frac{1}{2} \\ (2x_1, \frac{1}{2}(x_2+1)) \bmod 1, & \text{if } \frac{1}{2} \le x_1 < 1 \end{cases}$$

With initial condition $f^0(x) = \sqrt{\pi}\cos(2\pi x_2)$. How the Koopman operator of Baker's map acts on $f^0(x)$ is very simple: it doubles the frequency of the cosine wave at each iteration, as shown in figure 6. We further apply a diffusion operator with diffusivity D after every iteration to make the process diffusive. Just like in the mixing channel problem, we want to know how the variance

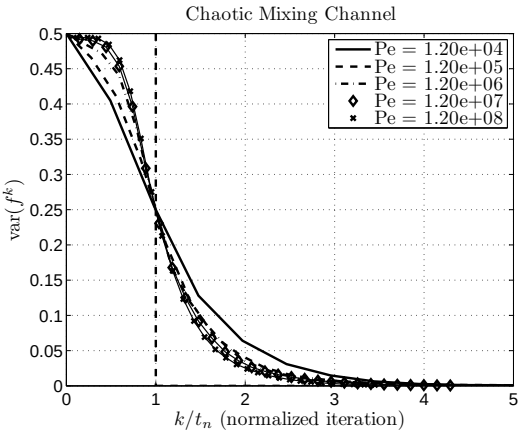

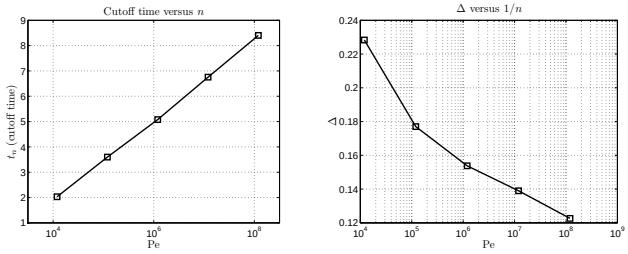

Figure 4. THE FIRST PLOT SHOW THE NORMALIZED TRAJECTORIES OF THE MICROFLUIDIC MIXING CHANNEL. IT CLEARLY PRESENTS A CUTOFF. THE SECOND PLOT SHOWS THE LINEAR RELATION BETWEEN CUTOFF TIME AND Pe, AND THE THIRD PLOT SHOWS THAT $\Delta^3_{\hat{B}}$ IS A DECREASING FUNCTION OF t_n, WHICH JUSTIFIES THE CUTOFF.

versus iteration looks like. This problem is analytically solvable:

$$f^k(x) = \sqrt{\pi}e^{-4\pi^2 D 2^{2k}}\cos(2\pi 2^k x_2) \text{ for } k = 1,2,\ldots$$

and the variance of $(f^k(x))$ is: $\text{var}(f^k(x)) = e^{-8\pi^2 D 2^{2k}}$ It is a doubly exponential function of k. We plot $\text{var}(f^k(x))$ in figure 7 with different D. One can easily tell from this figure that the set of trajectories presents a cutoff with cutoff time $t_n \sim -\log(D)$. The trajectories we see in the mixing channel simulation has the same tendency as the Baker's Map simulation. However, if we normalize the trajectories in figure 3 as we did in the second plot of figure 1, one would not see a cutoff. It is because that the relation $t_n \sim -\log(D)$ makes cutoffs can only be seen when the diffusion is extremely small, or Pe is very large. It is too expensive to simulate the mixing channel for $\text{Pe} > 10^{10}$. Hence in the next section, we numerically simulate another discrete map–Standard Map–to provide the numerical evidence of the chaotic map cutoff.

STANDARD MAP SIMULATION

We study Standard Map on T^2:

$$\begin{aligned} x_1' &= x_1 + x_2 + \varepsilon \sin 2\pi x_1 (\bmod 1), \\ x_2' &= x_2 + \varepsilon \sin 2\pi x_1 (\bmod 1). \end{aligned} \quad (10)$$

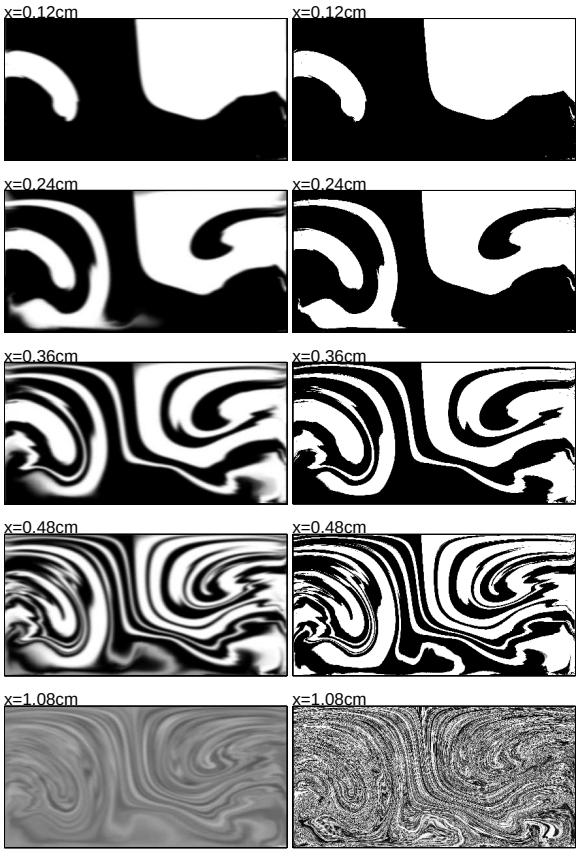

Figure 5. FOR Pe $= 1.2 \times 10^6$ (LEFT) AND 1.2×10^9 (RIGHT), WE PLOT THE CROSS-SECTIONS OF THE END OF THE 1ST TO THE 4TH CYCLE FOR BOTH CASES. THE BOTTOM TWO PLOTS SHOW THE CROSS-SECTIONS OF THE END OF THE 9TH CYCLE FOR BOTH CASES.

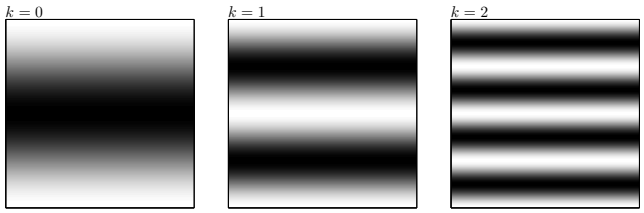

Figure 6. THE FIRST THREE ITERATIONS OF A FUNCTION $f^0 = \cos(2\pi x_2)$ ADVECTED BY BAKER'S MAP. IT SIMPLY DOUBLES THE FREQUENCY OF THE COSINE FUNCTION IN x_2 DIRECTION.

This map is known to be chaotic, where ε is a parameter that can be adjusted to change the behavior of the map. Various studies of how a point is advected by the map can be found, for example, in [18]. Here we mainly focus on how a scalar function is evolved by the map with the presence of small diffusion. Because this map is volume preserved, its invariant measure is uniform, there is no difference between evolving a scalar function and a probability distribution. However, there are a few words about the notion of cutoff we need to say:

1. When talking about Standard Map, due to the uniformity of the invariant distribution, the distance (9) is the same as the standard deviation of a function defined as $(f_n)_i = (\omega_n)_i/(\bar{\omega}_n)_i$ with mean 1. Thus in all of our simulations, we scale the mean of the initial functions to be 1 to fit the definition.
2. We scale the standard deviation of f^0 to be 1 in all the simulations and set M to be 1.
3. Standard Map is known to have some non-chaotic region when ε is not zero , so the distance d converge to a value $m \neq 0$.

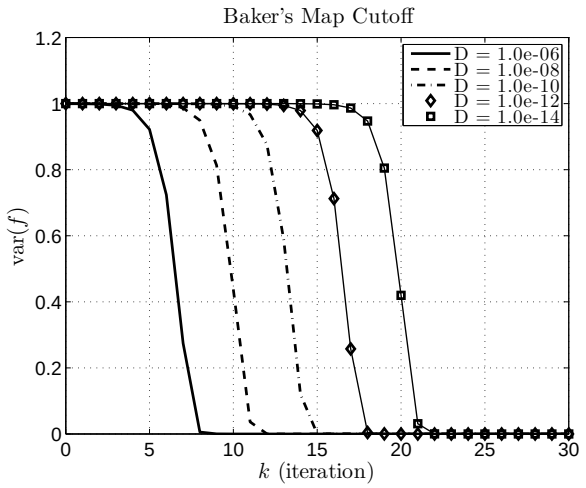

Figure 7. BAKER'S MAP CUTOFF.

The above points explain why we need to slightly modify the definition of cutoff phenomenon given by Diaconis.

To try to fit the definition of a cutoff, we perform the simulation with different n.For n from 2500^2 to 80000^2, the variance of f_n^k versus iteration plots using B_n and $\bar{B}_n$ as the Koopman operators are shown in the left of figures of 9 and 10. The tendency is clear: when n gets larger, the variance stays high ($M_B = M_{\bar{B}} = 1$) for more iterations and then drop rapidly to $m_B = 0.4521$ and $m_{\bar{B}} = 0.4498$, respectively–they do not drop to zero because there are unmixed "islands". The rapid dropping region also becomes slightly mild when n increases. To justify whether they satisfy the definition of cutoff, we let t_n equal the point that each trajectory passes through $(M_\star + m_\star)/2$, where $\star = \{B, \bar{B}\}$ and normalize all the trajectories by rescaling t_n to 1. The results are plotted in the right of figure 9 and 10. Although the normalized trajectories are very similar, one can still see that when n gets larger, the trajectory becomes sharper. In the upper plot of figure 11 we plot t_n versus $1/n$ in log scale and see two straight lines. Note that for both cases, we have $D \sim O(1/n)$. Hence this plot shows that the cutoff time is inversely proportional $\log(D)$. Just like we did in the mixing channel trajectories, we define the interpolating functions for the trajectories in the normalized plots of figures 9 and 10 to be $\beta_{B_n}(x)$ and $\beta_{\bar{B}_n}(x)$, where x represents the normalized iteration. The function they should converge to when $n \to \infty$ are $\beta_{B_\infty}(x)$ and $\beta_{\bar{B}_\infty}(x)$, respectively. We plot Δ_B^3 and $\Delta_{\bar{B}}^3$ versus t_n in the right of figure 11. This figure shows that when t_n increases, both Δ_B^3 and $\Delta_{\bar{B}}^3$ decay slightly slower than linear,

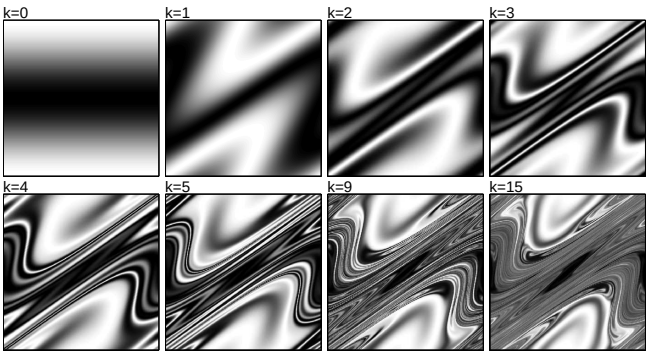

Figure 8. THIS FIGURE SHOWS THE FIRST EIGHT ITERATIONS OF f_n^k WHEN $f^0 = \cos(2\pi x_2)$ ADVECTED BY THE STANDARD MAP WTIH $\varepsilon = 0.3$, and $n = 500$.

but clearly when $n \to \infty$, Δ_B^3 and $\Delta_{\tilde{B}}^3$ are both going down, which strongly suggests that both sequences of Markov Chains present cutoffs.

CONCLUSION

We begin with the simulation of a microfluidic mixing channel which realizes chaotic mixing, and by observing the decay of the color variance on the cross-sections for different Pe's, we show that if we keep increasing Pe, the trajectories present a cutoff. We then provide the numerical evidence of cutoffs for the sequence of Markov Chains generated by approximating the Koopman operator of Standard Map. The notion of a cutoff is firstly brought from finite Markov Chain studies to the study of chaos, and we find not only it is suitable to characterize the behavior of chaotic map in the near zero-diffusion limit, but also it builds a bridge between large finite Markov Chain studies and chaotic maps.

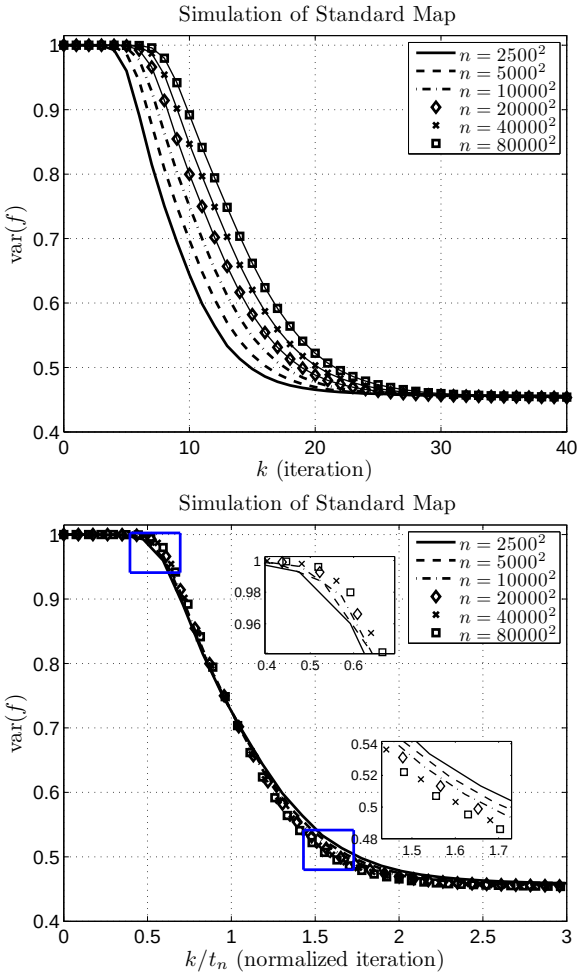

Figure 9. THE UPPER FIGURE SHOWS THE VARIANCE OF f_n^k VERSUS ITERATION TRAJECTORIES OF STANDARD MAP SIMULATION. WE USE $\varepsilon = 0.3$, $f^0 = \cos(2\pi x_2)$, AND NUMBER OF GRIDS VARIES FROM 2500^2 TO 80000^2. THE NORMALIZED PLOT IS SHOWN IN THE BOTTOM FIGURE. WE RESCALE THE ITERATION AXIS AND MAKE ALL TRAJECTORIES PASS THROUGH THE POINT $(1, 0.7260)$ TO OBSERVE THE CUTOFF. THE TWO SMALL PLOTS SHOW THE DETAIL VIEW OF THE CORNERS WHEN TRAJECTORIES HAVE SHARPE CHANGE.

REFERENCES

[1] Ottino, J. M., and Wiggins, S., 2004. "Introduction: Mixing in microfluidics". *Philosophical Transactions of the Royal Society A: Mathematical, Physical and Engineering Sciences,* **362**(1818), March, pp. 923–935.

[2] Voth, G. A., Haller, G., and Gollub, J. P., 2002. "Experimental measurements of stretching fields in fluid mixing". *Physical Review Letters,* **88**(25), June.

[3] Tsang, Y.-K., Antonsen, Jr., T. M., and Ott, E., 2005. "Exponential decay of chaotically advected passive scalars in the zero diffusivity limit". *Physical Review E,* **71**, June, p. 066301.

[4] Thiffeault, J.-L., and Childress, S., 2003. "Chaotic mixing in a torus map". *CHAOS,* **13**(2), June, pp. 502–507.

[5] Fereday, D. R., Haynes, P. H., Wonhas, A., and Vassilicos, J. C., 2002. "Scalar variance decay in chaotic advection and Batchelor-regime turbulence". *Physical Review E,* **65**(3), February, p. 035301.

[6] Mathew, G., Mezić, I., and Petzold, L., 2005. "A multi-scale measure for mixing". *Physica D,* **211**(1-2), November, pp. 23–46.

[7] Thiffeault, J.-L., 2004. "Scalar decay in chaotic mixing". In Transport in Geophysical Flows: Ten Years After, Proceedings of the Grand Combin Summer School.

[8] Haynes, P. H., and Vanneste, J., 2005. "What controls the decay of passive scalars in smooth flows?". *Physics of Fluids,* **17**, September, p. 097103.

[9] Cerbelli, S., Adrover, A., and Giona, M., 2003. "Enhanced diffusion regimes in bounded chaotic flows". *Physics Letters A,* **312**(5), June, pp. 355–362.

[10] Pierrehumbert, R. T., 2000. "Lattice models of advection-diffusion". *Chaos,* **10**(1), March, pp. 61–74.

[11] Froyland, G., 2001. "Extracting dynamical behaviour via Markov models". In *Nonlinear Dynamics and Statistics*.

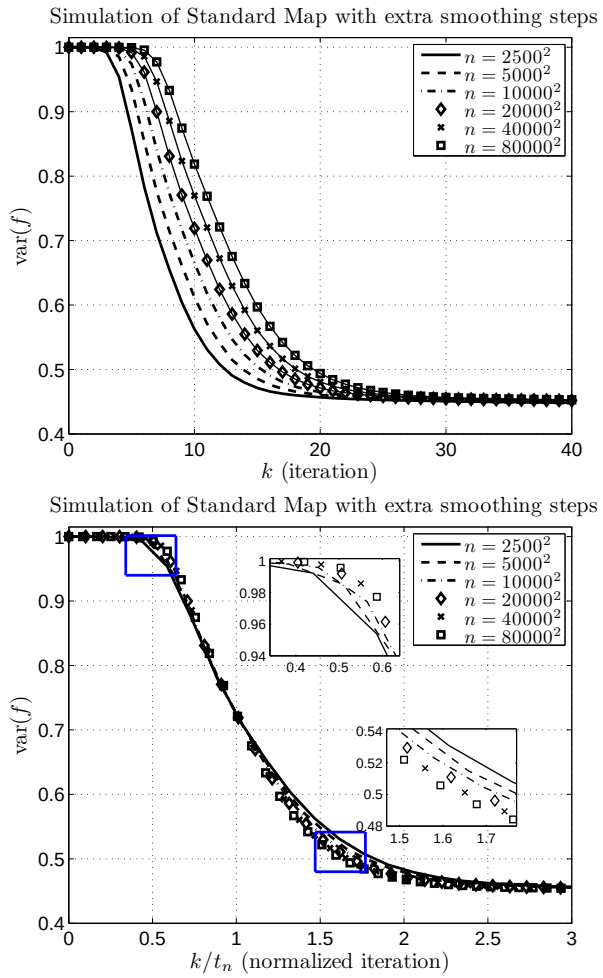

Figure 10. THE UPPER FIGURE SHOWS THE VARIANCE OF f_n^k VERSUS ITERATION TRAJECTORIES OF STANDARD MAP SIMULATION WHEN A SMOOTHING STEP IS ADDED AFTER EACH ITERATION. WE USE $\varepsilon = 0.3$, $f^0 = \cos(2\pi x_2)$, AND NUMBER OF GIRDS VARIES FROM 2500^2 TO 80000^2. THE NORMALIZED PLOT IS SHOWN IN THE BOTTOM PLOT. WE RESCALE THE ITERATION AXIS AND MAKE ALL TRAJECTORIES PASS THROUGH THE POINT $(1, 0.7249)$ TO OBSERVE THE CUTOFF. THE TWO SMALL PLOTS SHOW THE DETAIL VIEW OF THE CORNERS WHEN TRAJECTORIES HAVE SHARP CHANGE.

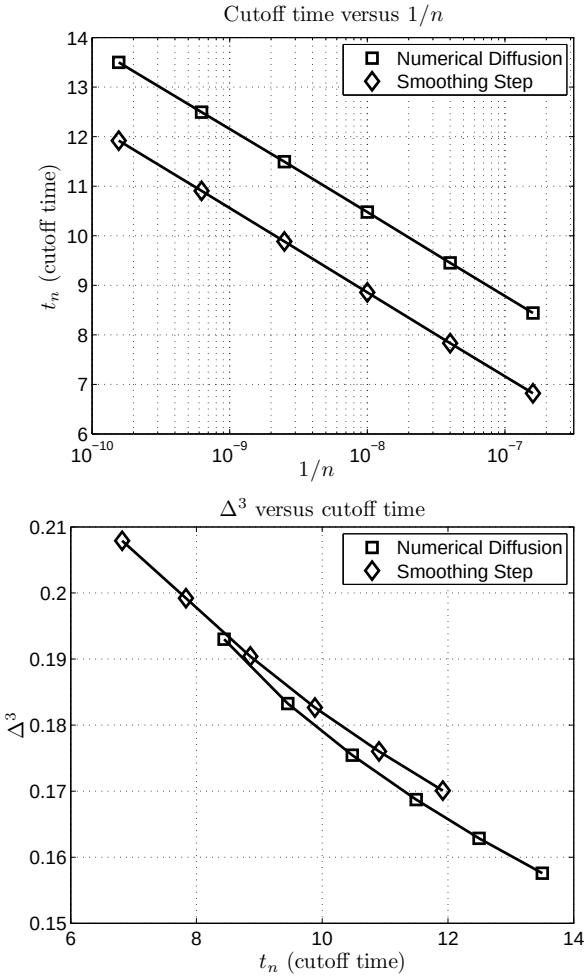

Figure 11. THE UPPER PLOT SHOWS HOW CUTOFF TIME t_n RELATES TO $1/n$ IN LOG SCALE. SINCE WE HAVE $D \sim O(1/n)$ FOR OUR SIMULATION STRATEGY, ONE CAN CONCLUDE THAT t_n IS INVERSELY PROPORTIONAL TO $\log(D)$. THE BOTTOM PLOT SHOWS HOW THE NORMALIZED TRAJECTORIES CONVERGE TO THEIR LIMITS. Δ^3 IS DEFINED IN EQUATION (8). BOTH CURVES PREDICT THAT WHEN t_n IS VERY LARGE, Δ^3 GOES DOWN, AND THE NORMALIZED TRAJECTORY WOULD LIKELY BECOME A STEP FUNCTION .

Birkhäuser, Basel, pp. 283–324.

[12] Diaconis, P., and Saloff-Coste, L., 2006. "Separation cutoffs for death and birth chain". *Annals of Applied Probability,* **16**(4), pp. 2098–2122.

[13] Diaconis, P., Graham, R. L., and Morrison, J. A., 1990. "Asymptotic analysis of a random walk on a hypercube with many dimensions". *Random Structures and Algorithms,* **1**(1), pp. 51–72.

[14] Yang, Z., Goto, H., Matsumoto, M., and Maeda, R., 2000. "Ultrasonic micromixer for microfluidic systems". In The Thirteenth Annual International Conference on Micro Electro Mechanical Systems, pp. 80–85.

[15] Stroock, A. D., Dertinger, S. K. W., Ajdari, A., Mezić, I., Stone, H. A., and Whitesides, G. M., 2002. "Chaotic mixer for microchannels". *Science,* **295**(5555), January, pp. 647–651.

[16] Ottino, J. M., and Wiggins, S., 2004. "Designing optimal micromixers". *Science,* **305**(5683), July, pp. 485–486.

[17] Liang, T.-C., and West, M., 2008. Optimized mixing in microfluidic channels. (In preparation).

[18] Ott, E., 2002. *Chaos in Dynamical Systems*. Cambridge University Press. ISBN 0521010845.